2005

Photoionization and electron-impact ionization of Xe3+

E. D. Emmons
University of Nevada - Reno

A. Aguilar
University of Nevada - Reno

M. F. Gharaibeh
University of Nevada - Reno

S. W. J. Scully
University of Nevada - Reno

R. A. Phaneuf
University of Nevada - Reno, phaneuf@unr.edu

See next page for additional authors

Authors

E. D. Emmons, A. Aguilar, M. F. Gharaibeh, S. W. J. Scully, R. A. Phaneuf, A. L. D. Kilcoyne, A. S. Schlachter, I. Álvarez, C. Cisneros, and G. Hinojosa

Photoionization and electron-impact ionization of Xe^{3+}

E. D. Emmons,* A. Aguilar,† M. F. Gharaibeh, S. W. J. Scully,‡ and R. A. Phaneuf
Department of Physics, MS 220, University of Nevada, Reno, Nevada 89557-0058, USA

A. L. D. Kilcoyne and A. S. Schlachter
Advanced Light Source, Lawrence Berkeley National Laboratory, MS 7-100, Berkeley, California 94720, USA

I. Álvarez, C. Cisneros, and G. Hinojosa
Centro de Ciencias Físicas, Universidad Nacional Autónoma de México, Apartado Postal 6-96, Cuernavaca 62131, Mexico
(Received 27 October 2004; published 8 April 2005)

Photoionization and electron-impact ionization of Xe^{3+} ions in the region of $4d$ inner-shell excitation-autoionization have been studied using interacting-beam spectroscopic techniques. Absolute cross sections for photoionization of Xe^{3+} have been obtained and the electron-impact spectrum has been normalized to previously published absolute data. The Xe^{3+} spectra show large contributions from $4d \rightarrow nf$ excitation-autoionization processes compared to the lower charge states of Xe due to the significant collapse of the nf wave functions into the ion core as the initial charge state of the ion is increased. In addition, a tentative value for the ionization potential of Xe^{3+} of 42.2 ± 0.2 eV was obtained.

DOI: 10.1103/PhysRevA.71.042704 PACS number(s): 32.80.Dz, 32.80.Hd

I. INTRODUCTION

Photoionization and electron-impact ionization of ions in the xenon ($Z=54$) isonuclear sequence, as well as the nearby elements in the periodic table, have been studied extensively over the past few decades. Many of these studies were stimulated by the early work of Ederer, where the $4d$ "giant resonance" phenomenon was first observed in photoionization of neutral Xe [1]. The giant-resonance behavior was first explained qualitatively by Cooper [2] using a nonhydrogenic single-particle model. An accurate quantitative explanation of the giant resonance was later given by calculations including correlation effects between the $4d$ electrons (see [3] and references therein). This giant resonance is described as a delayed onset of $4d \rightarrow \epsilon f$ direct photoionization, which leads to a broad, pronounced peak in the photoionization spectrum of neutral xenon centered about 32 eV above the $4d$ threshold [1]. The delayed onset is due to the greater ability of the higher-energy f waves to penetrate the centrifugal barrier, resulting in an increasing partial cross section for the $4d \rightarrow \epsilon f$ process [2]. In experiments that are capable of charge-analyzing the resulting photoions, the giant resonance appears in the double-photoionization channel since the $4d$ hole created decays with nearly unity probability by subsequent autoionization.

As the initial charge state of an ion in the xenon isonuclear sequence is increased, the giant resonance gradually decreases in importance, while discrete $4d \rightarrow nf$ excitation-autoionization processes become important. The giant resonance gradually becomes truncated as the $4d$ direct-ionization threshold increases in energy along the series [3]. As the charge state of the target is increased, the nf wave functions collapse into the core of the ion, and thus there is a significant overlap between them and the $4d$ wave function. A similar increase in the importance of the $4d \rightarrow nf$ discrete transitions as ionic charge is increased was first observed in photoionization along the barium ($Z=56$) isonuclear sequence by Lucatorto *et al.* [4]. A review of such studies is given by Kjeldsen *et al.* [5].

The giant-resonance phenomenon has also been shown to play a role in electron-impact ionization along the xenon isonuclear sequence. Achenbach *et al.* [6] observed a feature in electron-impact double ionization of Xe^+ whose magnitude and shape closely matched the giant resonance observed in photoionization of neutral Xe. As the charge state of the xenon ion increases, the giant resonance becomes less pronounced in electron-impact ionization as well as photoionization. Instead, much of the intensity is transferred into excitation-autoionization processes involving $4d \rightarrow nf$ transitions, as suggested by Gregory *et al.* [7]. Clearly, similar effects are occurring in both photoionization and electron-impact ionization in this sequence.

Photoionization along the xenon isonuclear sequence has been examined in several previous studies [8–13] covering the range of charge states from Xe^+ to Xe^{7+}. In addition, absolute photoionization cross sections were obtained for Xe^+ and Xe^{2+} [11,13]. In the present study, absolute cross sections with a total uncertainty of ±25% are obtained for photoionization of Xe^{3+} and the relative photoionization spectra are obtained with a resolution about an order of magnitude higher than in previous measurements. Electron-impact ionization has also been studied along the xenon isonuclear sequence [6,7,14–16], using setups capable of measuring absolute cross sections. In the current study, a fine energy-scanning mode was used to obtain high-statistical-precision spectroscopic data capable of resolving excitation-

*Electronic address: emmons@physics.unr.edu
†Present address: Atomic Physics Division, National Institute of Standards and Technology, Gaithersburg, MD 20899-8421, USA.
‡Present address: Department of Pure and Applied Physics, Queen's University, Belfast BT7 1NN, Northern Ireland.

autoionization steps. The electron-impact ionization spectrum covers the energy range of 70–90 eV, which is of interest due to strong $4d \rightarrow nf$ excitation-autoionization processes.

II. EXPERIMENTAL TECHNIQUES

The experiments were performed using two interacting-beam setups. They have been described in detail previously and will only be outlined briefly here. The photoionization study was performed using the ion-photon merged-beam apparatus located at beamline 10.0.1 of the Advanced Light Source (ALS) in Berkeley, California [17]. The electron-impact ionization experiment was performed using an electron-ion crossed-beam apparatus at the Multicharged Ion Research Facility at the University of Nevada, Reno [18].

The basic principle behind both experiments is to overlap an energetic ionizing beam (photons or electrons) with an ion beam and to examine the resulting products. After the ions exit the interaction region, the small fraction of product ions that have been further ionized is directed by static magnetic and electric fields to a single-particle detector. The primary ion beam, which has a lower charge state than the product ions, is deflected through a smaller angle by the fields and is collected in a Faraday cup. The electron or photon beam energy is scanned and a spectrum of the count rate versus energy is obtained. The ions in both experiments are produced by two different electron-cyclotron-resonance ion sources. The photon beam is generated by an undulator which supplies photons to beamline 10 at the ALS. The beam is monochromatized by a grazing-incidence spherical-grating monochromator with three interchangeable diffraction gratings that cover different energy ranges. The electron beam was obtained from an electron gun designed and constructed at Justus-Liebig University in Giessen, Germany [19].

As mentioned previously, in the present study absolute photoionization cross sections were obtained with a total uncertainty of 25%. This error was estimated by examining the scatter of different absolute cross-section measurements measured at the same photon energy but under different tuning conditions for the ion and photon beams. The largest source of uncertainty in the cross section is the measurement of the beam-overlap geometrical form factor. A detailed analysis of the contributions to the cross-section uncertainty using the present experimental setup is given in [17]. Note that in the present experiment a larger uncertainty is quoted than that in [17]. This is due to an increased estimate of the uncertainty in the measurement of the beam-overlap geometrical form factor.

Even with the relatively intense photon beams in the extreme ultraviolet–soft x-ray region produced by modern third-generation synchrotron light sources, it is desirable to perform experiments on photoionization of atomic ions using a merged-beam geometry because overlapping collinear beams of ions and photons over a path length of a few tens of centimeters significantly increases the signal over that obtained in a 90° crossed-beam geometry. By contrast, the intensity of the electron beams used in most experiments on electron-impact ionization of ions is sufficient to allow a crossed-beam geometry to be used. For comparison purposes, the intensity of the synchrotron radiation from the undulator on beamline 10 at the ALS is approximately 5×10^{13} photons/s at a resolving power $(E/\Delta E)$ of 1000 at a photon energy of 80 eV [20]. The electron gun used for the present study produced about 1 mA of current near 80 eV, which corresponds to about 6×10^{15} electrons/s. However, the electron energy resolution was not adjustable and was approximately 0.75 eV full width at half maximum at an electron beam energy of 80 eV, corresponding to a resolving power of about 100.

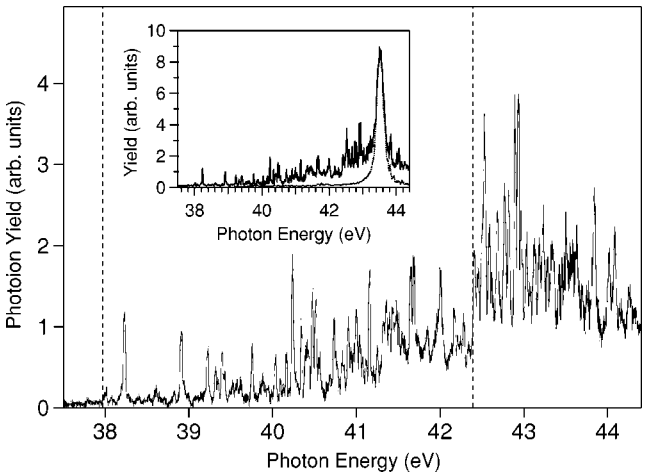

FIG. 1. Relative photoion yield of Xe^{4+} in the near-threshold region in photoionization of Xe^{3+}. Contamination from second-order lines for the $4d \rightarrow 4f$ transition band (centered near 87.0 eV in first order) has been subtracted (see text). The vertical dashed line at 42.39 eV marks a prominent level shift in the spectrum. The dashed line at 37.97 eV would be the onset of ionization of the $^2P_{3/2}$ metastable state if 42.39 eV were the ground-state ionization potential. A small feature at an energy of 37.8 eV leads to the conclusion that the ground-state ionization potential is likely actually near 42.2 eV. Inset: spectrum prior to subtraction of higher-order contamination. The upper curve shows the original spectrum and the lower curve shows the second-order feature that was subtracted to obtain the final spectrum.

III. EXPERIMENTAL RESULTS AND ANALYSIS

A. Photoionization of Xe^{3+}

1. Near-threshold region

Figure 1 shows the relative photoion yield of Xe^{4+} due to photoionization (PI) of Xe^{3+} in the near-threshold region for a photon energy resolution of 27 meV. This scan was performed in order to look for the ionization threshold and also to learn about possible metastable-state contamination of the ion beam. To our knowledge, the ionization potential of the $^4S_{3/2}$ ground state of Xe^{3+} is not accurately known. It is estimated, however, to have a value of 41 eV [21]. There was significant contamination of this spectrum due to features at twice the energy being observed in second order from the diffraction grating. These second-order features are due to $4d \rightarrow nf$ transitions, which have large cross sections. As will

be shown later, the $4d \rightarrow 4f$ transition band, which is centered at 87.0 eV, reaches a maximum cross section of approximately 280 Mb (1 Mb $= 1 \times 10^{-18}$ cm^2). Although absolute cross sections were not measured in this energy region, comparison of the features in this region to the $4d \rightarrow 5p$ excitations, for which absolute cross sections were measured, indicates that the cross section near threshold is of the order of 1–5 Mb. Thus, despite the low fraction of second- and higher-order radiation present in the photon beam, the $4d \rightarrow nf$ second-order features can have a dominant effect due to their much larger cross sections. This contamination was subtracted in Fig. 1 by shifting the $4d \rightarrow nf$ band onto the threshold scan and subtracting the higher-order features point by point. There may be significant errors in this subtraction around 43.5 eV, which is half the energy of the strong $4d \rightarrow 4f$ band at 87.0 eV. However, below 86.0 eV, the $4d \rightarrow 4f$ transitions are weak, so errors in the subtraction will be negligible below 43.0 eV. A method for filtering out higher-order radiation in the synchrotron beam was not available when the experiment was performed.

The analysis throughout this paper focuses on the main features of the spectra. The spectra are very complex due to the complicated angular momentum properties of Xe^{3+}, which has a half-filled $5p^3$ outer subshell in its ground-state electronic configuration. In the near-threshold region, the spectrum is significantly more complicated than the corresponding near-threshold spectrum for O^+ [22–24], which also has a half-filled outer p^3 subshell. Two factors likely contribute to this added complication. First, the fine-structure splitting of the states within the ground-state configuration is significantly larger in Xe^{3+} than in O^+. Thus, the fine-structure splitting is easily resolved in the present experiment, while it was not resolved in previous O^+ experiments. Second, the breakdown of *LS* coupling could allow additional transitions to become important.

A prominent level shift is evident in the spectrum at 42.39 eV, as indicated by the right-hand dashed vertical line in Fig. 1. This could possibly be a signature of the onset of strong resonances involving excitations starting from the ground state of Xe^{3+}. These are expected to be strong if a dominant portion of the ion beam is in the ground state. Due to the very dense resonance structure present, this level shift would likely be quite close to the threshold. An additional piece of evidence to support this hypothesis comes from the structure observed below this feature. Although the ionization potential of Xe^{3+} itself is not accurately known, the splittings of the states within the ground-state electronic configuration are well known from spectroscopic measurements [25]. The highest-lying state within the ground-state electronic configuration is the $^2P_{3/2}$ state, which is excited by 4.42 eV relative to the ground state. The $^2P_{3/2}$ state would thus have an ionization potential 4.42 eV lower than the ground-state ionization potential. If only states within the ground-state electronic configuration are populated significantly, the cross section would be zero for photon energies more than 4.42 eV below the ground-state ionization potential, i.e., photon energies below $42.39 - 4.42$ eV $= 37.97$ eV. Indeed, at photon energies below 37.97 eV (indicated by the left-hand dashed vertical line in Fig. 1) the photoion yield is quite small. However, a small feature is evident near 37.8 eV. It is therefore likely that the ionization potential of Xe^{3+} is slightly lower than 42.39 eV. It can be tentatively assigned a value of 42.2 ± 0.2 eV.

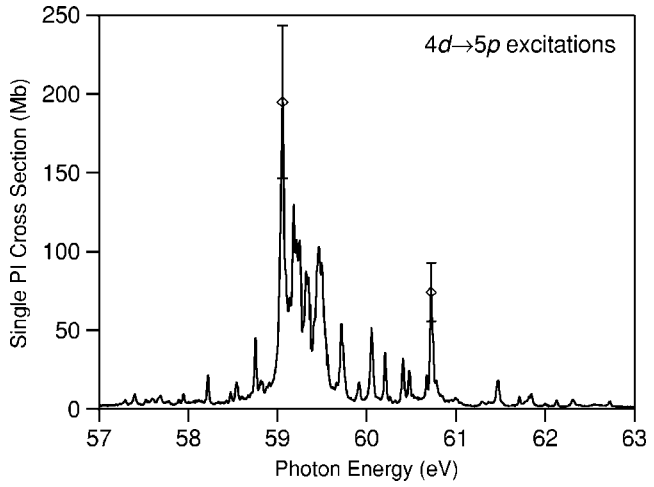

FIG. 2. Single-photoionization cross sections for the $4d \rightarrow 5p$ transitions in Xe^{3+} measured with an energy resolution of 20 meV. The open diamonds with error bars show the uncertainty in the absolute cross section measurements. The statistical (counting) uncertainty is as low as 0.9%.

2. $4d \rightarrow 5p$ excitation-autoionization

Figure 2 shows the absolute single-photoionization cross section as a function of photon energy in the range of 57–63 eV. The photon energy resolution in this measurement was 20 meV. The resonances in this energy region are due to transitions within the $4d \rightarrow 5p$ band. The strongest resonances appear at an energy just above 59 eV. The corresponding transitions in Xe^+ are centered around 55–56 eV while those for Xe^{2+} are centered around 57–58 eV [13]. The spectrum is more complicated than those for Xe^+ and Xe^{2+} due to the involvement of the $4d^{10}5p^3$ initial and $4d^9 5p^4$ intermediate configurations, which have complicated angular momentum properties. In addition, the large photon flux and energy resolution available at the ALS allows even the smaller transitions in the band to be observed and resolved.

The integrated oscillator strength f for this transition band was obtained using the formula [5]

$$f = (9.11 \times 10^{-3}) \int_{E_1}^{E_2} \sigma(E) dE,$$

where f is a dimensionless quantity, $\sigma(E)$ is the cross section in megabarns, E is the photon energy in eV, and E_1 and E_2 are the energy limits of the range for which the oscillator strength is to be determined. The value obtained for Xe^{3+} is 0.80, which can be compared to the corresponding values of 0.12 and 0.22 for Xe^+ and Xe^{2+}, respectively [13]. Clearly these transitions are becoming more significant as the ion charge state is increased.

3. $4d \rightarrow nf$ excitation-autoionization

Figure 3 shows absolute single-photoionization cross sections for Xe^{3+} in the energy range of 83–103 eV. This spec-

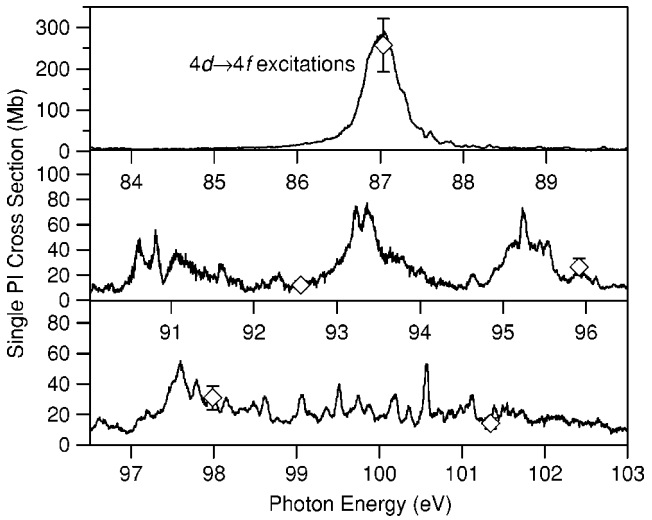

FIG. 3. Single-photoionization cross sections for the $4d \rightarrow nf$ transitions in Xe^{3+} measured with an energy resolution of 51 meV. The diamonds with associated error bars show individual absolute cross-section measurements that were used to normalize the spectrum. The statistical (counting) uncertainty is as low as 1.1%.

trum was obtained at a photon energy resolution of 51 meV. In this region there are strong transition bands due to $4d \rightarrow nf$ excitation-autoionization processes, with a probable extra contribution coming from $4d \rightarrow np, n \geq 6$, transitions. The strongest transition band is centered at 87.0 eV and has a maximum cross section of 280 Mb. It is due to transitions from the $4d$ subshell to the $4f$ subshell. Due to the broad nature of these transition bands, the maximum cross section observed is not significantly affected by the photon energy resolution. The integrated cross section contained in the single ionization channel for the $4d \rightarrow nf$ excitation bands gives an oscillator strength of 4.84. This can be compared to total oscillator strengths in the $4d \rightarrow nf$ excitation channels of 0.55 for Xe^{2+} and 0.04 for Xe^{+}.

Clearly, a significant collapse of the nf wave functions into the inner potential well is occurring as the ionic charge state is increased from Xe^{2+} to Xe^{3+}. In Xe^{3+} the majority of the oscillator strength is associated with discrete excitation channels, as opposed to the giant resonance. As shown in the work of Bizau *et al.* [12], the giant resonance shows up only weakly in photoionization of Xe^{4+}, and in Xe^{5+} and higher charge states it was unmeasurable.

4. Double ionization

Figure 4 shows absolute double-photoionization cross sections for Xe^{3+} in the energy range of 93–115 eV. The region of the spectrum below 104 eV was measured with a resolution of 51 meV, while the higher-energy region was measured with a nominal resolution of 100 meV. The higher-energy region was measured with a lower resolution due to its lack of structure. Due to this lack of structure it was not necessary or possible to determine the true resolution, as opposed to the nominal one. The resonances in the lower half of the spectrum are due to $4d \rightarrow nf$ excitations followed by emission of two Auger electrons. A likely reaction pathway for this process is

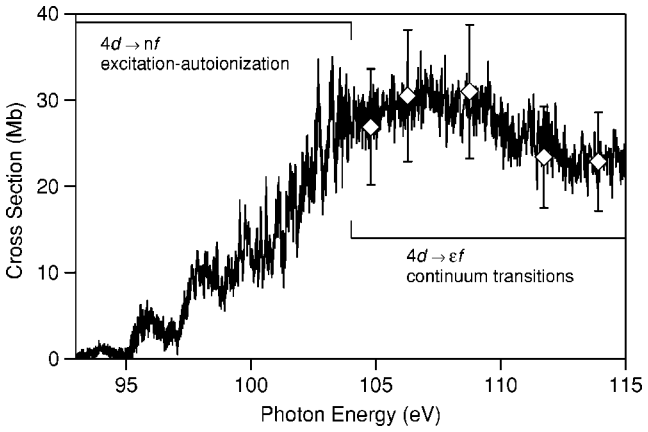

FIG. 4. Double-photoionization cross sections for the $4d \rightarrow nf, \epsilon f$ transitions in Xe^{3+}. The data below 104 eV show discrete structure due to $4d \rightarrow nf$ excitation-autoionization. The data above 104 eV show the discrete $4d \rightarrow \epsilon f$ transitions that form the "giant" resonance. The diamonds with associated error bars show individual absolute cross-section measurements that were used to normalize the spectrum. Typical statistical (counting) uncertainties are approximately 7%.

$$Xe^{3+}(4d^{10}5s^25p^3) + \gamma \rightarrow Xe^{3+}(4d^95s^25p^3nf)$$

$$\hookrightarrow Xe^{4+}(4d^{10}5s5p^3) + e^-$$

$$\hookrightarrow Xe^{5+}(4d^{10}5s^25p) + 2e^-. \quad (1)$$

This pathway competes with the pathway leading to single ionization

$$Xe^{3+}(4d^{10}5s^25p^3) + \gamma \rightarrow Xe^{3+}(4d^95s^25p^3nf)$$

$$\hookrightarrow Xe^{4+}(4d^{10}5s^25p^2) + e^-. \quad (2)$$

The difference between these pathways is whether or not the $5s$ electrons become involved and create an additional inner-shell hole that allows for emission of a second Auger electron. The double-ionization resonances shown in Fig. 4 correspond to resonances at the same energy in Fig. 3, which shows that they are due to excitation of the same intermediate excited state followed by decay along these two different pathways. The relative cross sections indicate that the branching ratios favor single autoionization over double autoionization.

The various $4d$ direct-ionization thresholds occur around an energy of about 104 eV. Above this energy, continuum $4d \rightarrow \epsilon f$ transitions comprising the giant resonance are important. The maximum cross section at the peak of the giant resonance is $\approx$30 Mb. This is consistent with measurements for ions in the lower charge states in the xenon isonuclear sequence. Essentially, the giant resonance is becoming truncated as the $4d$ ionization potential increases in energy along the isonuclear sequence. The integrated oscillator strength for the portion of the discrete $4d \rightarrow nf$ excitation processes leading to double ionization is 1.04. This value was obtained using the approximation that below 104.0 eV all of the os-

TABLE I. Table of oscillator strengths for different configurations in the xenon isonuclear sequence. The values for Xe, Xe^+, and Xe^{2+} are from Andersen *et al.* [13].

Target	$4d \rightarrow 5p$ excitations	$4d \rightarrow nf$ excitations	$4d \rightarrow \epsilon f$ continuum	Total
Xe	0	0	10.19	10.19
Xe^+	0.12	0.04	9.48	9.64
Xe^{2+}	0.22	0.55	8.74	9.51
Xe^{3+}	0.80	5.88	3.8	10.5

cillator strength is in discrete excitations, while above 104.0 eV all of the oscillator strength contributes to the continuum giant resonance.

Table I summarizes the oscillator strengths for the different types of ionization processes along the xenon isonuclear sequence. The values for Xe, Xe^+, and Xe^{2+} are tabulated by Anderson *et al.* [13]. In all cases the total $4d$ oscillator strength is consistent with 10, the number of $4d$ electrons as predicted by the Thomas-Riche-Kuhn (TRK) sum rule. The data in Table I show that there is a significant collapse of the nf wave functions into the inner well of the ion as the initial charge state is increased going from Xe^{2+} to Xe^{3+}. This increases the importance of the discrete transitions and decreases the importance of the giant resonance. Kjeldsen *et al.* [5] present an extended table of this type covering low charge states ($q<3$) of ions of elements from I ($Z=53$) to Ba ($Z=56$). The present study adds a triply charged ion to this compilation. Of these ions, Xe^{3+} has the largest contribution due to discrete $4d$ excitation-autoionization processes. Indeed, the collapse of nf wave functions into the inner well is quite dramatic, compared to the more gradual collapse for ions in the lower charge states.

B. Electron-impact ionization of Xe^{3+}

Figure 5 shows single-electron-impact ionization (EII) cross-section measurements for Xe^{3+}. The electron energy resolution of the spectrum is approximately 0.75 eV. The data were taken in a fine energy-scanning mode and only relative cross sections were obtained. They have been normalized to the absolute cross-section measurements of Gregory *et al.* [7]. A distinct step is evident in the cross section at 83 eV. This is likely due to the onset of $4d \rightarrow 4f$ excitation-autoionization. The corresponding process in photoionization does not become significant until just below 87 eV. There are several possible reasons for the differences between photon- and electron-induced ionization. First, according to theoretical predictions [14], the $4d \rightarrow 5d$ transition band begins at an energy slightly lower than the $4d \rightarrow 4f$ transition band. $4d \rightarrow 5d$ transitions should be unobservable in the photoionization spectrum, since the parity of the ionic state does not change as required by the electric-dipole selection rules. However, these transitions can occur in electron-impact ionization since the electric-dipole selection rules are relaxed due to the exchange mechanism. Another reason that this step could come at a lower energy than the 87 eV peak

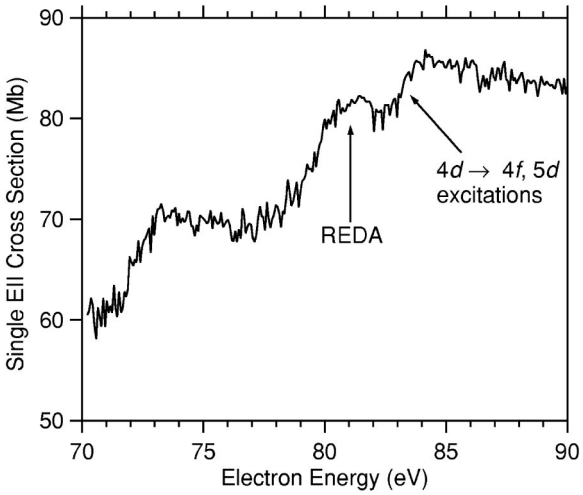

FIG. 5. Electron-impact single-ionization cross sections for the $4d \rightarrow nf, \epsilon f$ transitions in Xe^{3+} measured with an energy resolution of 0.75 eV.

observed in the photoionization spectrum is that lower-energy transitions within the $4d \rightarrow 4f$ excitation band could be relatively more important in electron-impact ionization.

There is another feature in the electron-impact spectrum near 80 eV. It is unclear from the present spectrum if this feature is a step due to excitation-autoionization or a resonance due to a process such as resonant recombination followed by double autoionization. However, unpublished high-statistical-precision data of Müller confirm that there is indeed resonance structure at 80 eV [26]. The likely origin of this resonance structure is recombination with excitation which leads to an excited state of Xe^{2+} with the configurations $4d^9 5s^2 5p^3 4fnl$. Resonant-recombination processes that populate these configurations would appear just lower in energy than the $4d \rightarrow 4f$ excitation-autoionization threshold. Population of these states would then lead to net single ionization following the emission of two Auger electrons. This could occur via the reaction

$$\begin{aligned} Xe^{3+}(4d^{10}5s^2 5p^3) + e^- &\rightarrow Xe^{2+}(4d^9 5s^2 5p^3 4fnl) \\ &\hookrightarrow Xe^{3+}(4d^{10}5s5p^3 4f) + e^- \\ &\hookrightarrow Xe^{4+}(4d^{10}5s^2 5p^2) + 2e^-, \end{aligned} \tag{3}$$

and through other similiar pathways. This reaction is known as the resonant excitation–double-autoionization process [27], since two Auger electrons are emitted sequentially. An alternative process known as resonant excitation–auto-double-ionization is also possible [27] and would be indistinguishable in the present measurements. In this process, two Auger electrons are emitted simultaneously in one decay step. It is unlikely, however, that this process contributes significantly to the observed resonances since it is a second-order process requiring a high degree of correlation among the excited electrons.

IV. SUMMARY AND CONCLUSIONS

Spectroscopic measurements for photoionization and electron-impact ionization of Xe^{3+} in the region of inner-shell $4d$ excitation-ionization have been presented. In the energy range below 150 eV, indirect $4d \rightarrow 5p,nf$ $(n \geqslant 4)$ excitation-autoionization is much more important than in the lower-charged members of the isonuclear sequence. This is attributed to the collapse of the nf wave functions into the inner potential well of the ion core as the initial ion charge state is increased, resulting in increased overlap with the $4d$ wave functions. Due to this effect, strong spectroscopic signatures of discrete excitation-autoionization processes are observed in both photoionization and electron-impact ionization of Xe^{3+}. It is evident that similar excitations occur in photoionization and electron-impact ionization of Xe^{3+}. However, additional processes contribute to electron-impact ionization, such as resonant recombination followed by double autoionization as well as the excitation of nondipole transitions.

A detailed theoretical examination of the spectra presented in this paper would certainly be helpful, particularly for the case of photoionization where a very complicated resonance structure is observed. Indeed, the present experimental spectra are valuable for benchmarking electron-impact ionization and photoionization calculations such as those presented in [14,28]. Efforts under way to perform extreme ultraviolet lithography using a xenon-based laser-produced plasma as a light source require such calculations and experimental data to test the calculations. Gilleron *et al.* [28] contains such an analysis for the xenon isonuclear sequence; however, Xe^{3+} is not treated in detail.

Complementary studies of photoionization and electron-impact ionization are a powerful tool for studying atomic structure and dynamics. Since both areas of study have matured to a significant extent, using them in tandem is now feasible. However, the resolution of the photoionization experiments is generally much better than that obtained in electron-impact ionization studies. Experiments on higher-energy synchrotron-radiation beamlines, such as those of Oura *et al.* [29–31], would be useful because at these energies photoionization resonances are more widely separated and the energy resolution would be comparable in photoionization and electron-impact ionization measurements.

ACKNOWLEDGMENTS

This work was supported by the U.S. Department of Energy, Division of Chemical Sciences, Biosciences, and Geosciences under Grant No. DOE-FG02-03ER15424. A.A. and M.F.G. acknowledge support from the ALS. We thank A. Müller for providing us with his unpublished electron-impact ionization data for comparison and J. D. Bozek and B. Rude for assistance with the photon energy calibration for the photoionization experiment.

[1] D. Ederer, Phys. Rev. Lett. **13**, 760 (1964).
[2] J. Cooper, Phys. Rev. Lett. **13**, 762 (1964).
[3] K. Cheng and W. Johnson, Phys. Rev. A **28**, 2820 (1983).
[4] T. Lucatorto, T. McIlrath, J. Sugar, and S. Younger, Phys. Rev. Lett. **47**, 1124 (1981).
[5] H. Kjeldsen, P. Andersen, F. Folkmann, J. Hansen, M. Kitajima, and T. Andersen, J. Phys. B **35**, 2845 (2002).
[6] C. Achenbach, A. Müller, E. Salzborn, and R. Becker, Phys. Rev. Lett. **50**, 2070 (1983).
[7] D. Gregory, P. Dittner, and D. Crandall, Phys. Rev. A **27**, 724 (1983).
[8] M. Sano, Y. Itoh, T. Koizumi, T. Kojima, S. Kravis, M. Oura, T. Sekioka, N. Watanabe, Y. Awaya, and F. Koike, J. Phys. B **29**, 5305 (1996).
[9] N. Watanabe *et al.*, J. Phys. B **31**, 4137 (1998).
[10] T. Koizumi *et al.*, Phys. Scr., T **73**, 131 (1997).
[11] Y. Itoh, A. Ito, M. Kitajima, T. Koizumi, T. Kojima, H. Sakai, M. Sano, and N. Watanabe, J. Phys. B **34**, 3493 (2001).
[12] J.-M. Bizau *et al.*, Phys. Rev. Lett. **84**, 435 (2000).
[13] P. Andersen, T. Andersen, F. Folkmann, V. Ivanov, H. Kjeldsen, and J. West, J. Phys. B **34**, 2009 (2001).
[14] D. Griffin, C. Bottcher, M. Pindzola, S. Younger, D. Gregory, and D. Crandall, Phys. Rev. A **29**, 1729 (1984).
[15] C. Achenbach, A. Müller, E. Salzborn, and R. Becker, J. Phys. B **17**, 1405 (1984).
[16] A. Müller, C. Achenbach, E. Salzborn, and R. Becker, J. Phys. B **17**, 1427 (1984).
[17] A. Covington *et al.*, Phys. Rev. A **66**, 062710 (2002).
[18] R. Rejoub and R. Phaneuf, Phys. Rev. A **61**, 032706 (2000).
[19] M. Stenke, K. Aichele, D. Hathiramani, G. Hofmann, M. Steidl, R. Völpel, and E. Salzborn, Nucl. Instrum. Methods Phys. Res. B **98**, 573 (1995).
[20] A. Aguilar, Ph.D. thesis, University of Nevada, Reno, 2003.
[21] G. Rodriguez, P. Indelicato, J. Santos, P. Patte, and F. Parente, At. Data Nucl. Data Tables **86**, 117 (2004).
[22] A. Covington *et al.*, Phys. Rev. Lett. **87**, 243002 (2001).
[23] A. Aguilar *et al.*, Astrophys. J., Suppl. Ser. **146**, 467 (2003).
[24] H. Kjeldsen, B. Kristensen, R. Brooks, F. Folkmann, H. Knudsen, and T. Andersen, Astrophys. J., Suppl. Ser. **138**, 219 (2002).
[25] J. R. Almandos, F. Bredice, M. Gallardo, C. Pagan, H. D. Rocco, and A. Trigueros, Phys. Rev. A **43**, 6098 (1991).
[26] A. Müller (private communication).
[27] G. Hofmann, A. Müller, K. Tinschert, and E. Salzborn, Z. Phys. D: At., Mol. Clusters **16**, 113 (1990).
[28] F. Gilleron, M. Poirier, T. Blenski, M. Schmidt, and T. Ceccotti, J. Appl. Phys. **94**, 2086 (2003).
[29] M. Oura *et al.*, Phys. Rev. A **63**, 014704 (2001).
[30] M. Oura, H. Yamaoka, K. Kawatsura, T. Hayaishi, J. Kimata, T. Kojima, M. Kimura, T. Sekioka, and M. Terasawa, Rev. Sci. Instrum. **71**, 1206 (2000).
[31] H. Yamaoka, M. Oura, K. Kawatsura, T. Hayaishi, T. Sekioka, A. Agui, A. Yoshigoe, and F. Koike, Phys. Rev. A **65**, 012709 (2002).